Phase behavior of the generalized chiral Lebwohl-Lasher model in bulk and confinement

P. Elsässer and A. Kuhnhold[*]

Institute of Physics, University of Freiburg, 79104 Freiburg (Breisgau), Germany

One of the simplest models that is used to study the isotropic-nematic tranition in liquid crystalline systems is the Lebwohl-Lasher model. Several extensions of this model further enhanced its applicability. We combine two of these extensions (a generalization and the inclusion of a chiral term) and study the phase behavior and the nature of phase transitions of the resulting generalized chiral Lebwohl-Lasher model using Monte Carlo simulations. We find that the type (and even the existence) of the transition depends on the combination of the width of the interaction potential, the strength of the chiral part of the interaction, and the geometry of the system. As well, the pitch of the cholesteric bulk phase changes on approaching the phase transition if the interaction width differs from the one of the original Lebwohl-Lasher model. Thus, we identify parameter combinations that allow one to tune the properties of the ordered phase and the nature of the order-disorder transition.

I. INTRODUCTION

A central topic of studies regarding liquid-crystalline (LC) systems is their phase behavior and the nature of phase transitions. To better understand the properties of LC systems, several models have been introduced that facilitate the theoretical treatment (analysis and computer simulation) of such systems [1]. In this paper we focus on one of them: the Lebwohl-Lasher model [2]. We will use a specific version of this model and study the influence of different combinations of parameters on the phase behavior.

In many cases (experimental systems and theoretical models), the orientational order-disorder (nematic-to-isotropic) transition in bulk systems is found to be a first-order transition. However, the microscopic details and the geometry of a system can alter the behavior. This is studied and discussed extensively for the Lebwohl-Lasher (LL) model: anisotropic particles are fixed to a simple cubic lattice and interact with their nearest neighbors via

$$E_{ij} = -\varepsilon P_2(\hat{\omega}_i \cdot \hat{\omega}_j) = -\varepsilon P_2(\cos(\theta_{ij})), \quad (1)$$

with a positive coupling constant ε, the orientations of the two particles $\hat{\omega}_i$ and $\hat{\omega}_j$, the angle between their long axes θ_{ij}, and the second Legendre polynomial $P_2(x)$. This model system undergoes a weak first-order isotropic-nematic (IN) transition in the three-dimensional bulk case [2–11]. In contrast, for the quasi-two-dimensional case (2D lattice with 3D particle orientations), the debate about the presence and the nature of an orientational order-disorder transition is still ongoing [8,12–26]; cf. Table II below.

The situation is clearer for the generalized Lebwohl-Lasher (gLL) model introduced by Vink [27]: the "sharpness" of the interaction is tuned by a parameter p:

$$E_{ij} = -J|\cos(\theta_{ij})|^p. \quad (2)$$

For $p = 2$ and the coupling constant set to $J = 3/2\,\varepsilon$, the gLL model reduces to the original LL model (with an additional constant shift of the energy value). With increasing p, the "strength" of the first-order bulk transition increases, and the transition in the two-dimensional case can be tuned from no transition to continuous transition to first-order transition [17,18].

The original LL model has been extended as well to account for the chiral nematic phase. This phase is also called the cholesteric phase, and its characteristic is that the nematic director (the common orientation of particles) rotates along an axis. The resulting cholesteric helix is described by the cholesteric pitch, which is one of the main quantities of interest in these systems because it is related to the optical properties of the macroscopic sample. The chiral Lebwohl-Lasher (cLL) model (named in this way by Memmer *et al.* [28,29], but also used by other authors, like Saha *et al.* [30,31], Luckhurst *et al.* [32], or Skutnik *et al.* [33]) includes a chiral interaction term in the pair potential

$$E_{ij} = -J(\hat{\omega}_i \cdot \hat{\omega}_j)^2 - K[(\hat{\omega}_i \times \hat{\omega}_j) \cdot \hat{r}_{ij}](\hat{\omega}_i \cdot \hat{\omega}_j), \quad (3)$$

where $\hat{r}_{ij}$ is the unit vector between the particles' positions. To simplify the simulations and fix the orientation of the cholesteric helix, the particle axes in these systems are often confined to a plane. With this, the orientational order-disorder (chiral nematic-to-isotropic) transition is found to be of second order or higher for K sufficiently large [28,32]. With the special form of Eq. (3), the cholesteric pitch only depends on the ratio K/J but not on the temperature of the system. This originates from the sharpness parameter p of the achiral part being 2. With the paper at hand, we combine the two generalizations (adding a chiral term and adjusting the interaction sharpness) and describe the system behavior with respect to the cholesteric pitch and the nature of the isotropic-to-cholesteric (IN*) transition for different geometries. We present results for parameter combinations that lead to a variation of the system behavior. An explicit mapping or

_____
*anja.kuhnhold@physik.uni-freiburg.de

comparison to specific systems is not the scope of this paper, but it may guide future studies about modeling cholesteric systems.

The paper is structured as follows: In Sec. II we introduce the generalized chiral model and describe the simulation techniques we use and the analysis of the relevant observables. The Results section begins with a discussion of the system in the three-dimensional bulk geometry in Sec. III A. We then briefly add our results to the debate about the nature of the IN transition in the quasi-two-dimensional case in Sec. III B. Next, in Sec. III C we describe how the model behaves when confined to a slab of three layers. Finally, we close the Results section with the study of the transition between the thin film and bulk behavior in Sec. III D and summarize our findings in Sec. IV.

II. MODEL AND SIMULATIONS

The chiral molecules that form the liquid crystalline system interact via a generalized chiral Lebwohl-Lasher (gcLL) interaction, which is a modification of the Lebwohl-Lasher (LL) model that is used for studying phase transitions of liquid crystals [2]. Each molecule within the system is described by a three-dimensional unit vector $\hat{\omega}_i$, which points in the direction of the long axis of the molecule. These vectors are fixed in a simple cubic lattice with lattice constant λ and $L_x \times L_y \times L_z = N$ lattice sites. Only nearest neighbor (n.n.) interactions are considered, and the pair interaction between molecule i and j is given by

$$E_{ij} = -J|\hat{\omega}_i \cdot \hat{\omega}_j|^p - K[(\vec{\omega}'_i \times \vec{\omega}'_j) \cdot \hat{r}_{ij}](\vec{\omega}'_i \cdot \vec{\omega}'_j). \quad (4)$$

The original LL model consists of only the first term with $p = 2$; the generalization to arbitrary p was introduced and studied by Vink and Fish [17,18,27]. With this achiral part, whose contribution to the total interaction energy is controlled by the factor J, a parallel alignment of the vectors is favored. In the second term (the chiral contribution) with the factor K the energetically lowest state is reached by twisting the vectors against each other. $\vec{r}_{ij}$ is the vector between the positions of two molecules in units of the lattice constant λ, and $\hat{r}_{ij}$ is the respective unit vector. In comparison to the cLL model used by other authors [28–32], we include only the x and y components of the orientations in the chiral contribution, i.e., we use $\vec{\omega}'_{i,j}$, which is the projection of $\hat{\omega}_{i,j}$ onto the xy plane. In this way, we do not have to confine the orientations to two dimensions to be able to control the direction of the helix axis in the cholesteric phase and, at the same time, allow for a proper three-dimensional disordered phase. Another method of prescribing the cholesteric axis while allowing for three-dimensional orientations was applied in Ref. [33]: They use the full orientation of $\vec{\omega}$ and multiply the chiral contribution term with $(\hat{r}_{ij} \cdot \hat{e}_z)^2$ so that the chiral interaction also acts only between particles in different planes. We assume that this difference will affect only the high-temperature regime, where the particles rotate out of plane; the chiral contribution in our system is then weaker because we consider the projections to the plane. In the following we will call $K^* = KJ^{-1}$ chirality parameter because the ratio of K and J governs the strength of the twist in the cholesteric phase. The system's energy $E^* = EJ^{-1} = \sum_{n.n.} E_{ij}J^{-1}$ and the inverse temperature

$\beta^* = \beta J = J/k_B T$, with the Boltzmann constant k_B, are as well made dimensionless by including the prefactor J. The number of molecules equals the number of lattice sites.

The simulation box has periodic boundary conditions in the x and y directions. We simulate thin films by using free surfaces in the z direction, while in bulk systems, self-determined boundary conditions are applied [34]. For those, periodic images of the simulation box are used, like for "normal" periodic boundaries, but all orientations in the periodic images are rotated by some angle ϕ_B within the xy plane. This angle is determined by an additional Monte Carlo move, i.e., besides the attempts to rotate the molecular orientations (N trials per MC sweep), an attempt to change ϕ_B is taken once per MC sweep. With these boundaries, it is possible to find the equilibrium cholesteric pitch of the system even if this pitch is not commensurate with the height of the simulation box.

We use Metropolis [35] and transition-matrix Wang-Landau (TMWL) Monte Carlo [36,37] simulations. The Metropolis algorithm simulates systems in the NVT ensemble by creating a Markov chain of states Γ that are visited according to their Boltzmann weight $P_B(\Gamma) \propto \exp[-\beta E(\Gamma)]$. The TMWL, on the other hand, performs a random walk in energy space with the aim to visit all energy states equally often. This allows one to simulate first-order phase transitions more efficiently. In Metropolis simulations, it is very unlikely to cross a large (free) energy barrier, such as occurs between two coexisting phases at a first-order transition. For the TMWL algorithm, such an energy barrier does not present a problem. But suppose one is mainly interested in measuring observables in a phase space region without phase transitions. In that case, it is convenient to use the standard Metropolis algorithm because one does not gain much by visiting all available energy states. We will focus on results obtained with the transition-matrix Wang-Landau algorithm and briefly summarize it in the following. The TMWL algorithm consists of two parts: a "prepare" and a "collect" stage. In each step, a rotation is proposed for a randomly chosen molecule. This new state is accepted with probability

$$h(o \rightarrow n) = \min\left(\frac{G(E_o^*)}{G(E_n^*)}, 1\right), \quad (5)$$

where E_o^* is the energy of the old state and E_n^* is the energy of the newly proposed state. $G(E^*)$ is the density of states which is connected to the energy probability distribution $P(E^*)$ by $P(E^*) \propto G(E^*) \exp(-E^*\beta^*)$.

At the beginning of the "prepare" stage, $G(E^*)$ is not yet known and set to $G(E^*) = 1$. Each time an energy bin is visited, the corresponding $G(E^*)$ is multiplied by some factor $f \geqslant 1$. Simultaneously, we measure the elements of the transition matrix $T(E_o^* \rightarrow E_n^*)$ which are the numbers of proposed moves from state E_o^* to state E_n^*. These allow one as well to calculate the density of states via [37]

$$\frac{G(E_o^*)}{G(E_n^*)} = \frac{\Omega(E_n^* \rightarrow E_o^*)}{\Omega(E_o^* \rightarrow E_n^*)}, \quad (6)$$

where $\Omega(E_i^* \rightarrow E_j^*) = T(E_i^* \rightarrow E_j^*)/\sum_{E_j^*} T(E_i^* \rightarrow E_j^*)$ is the probability for the proposition of a move from one state E_i^* to another E_j^*. Additionally, a histogram $H(E^*)$ of visited energy bins is filled. The energy binning for the histogram and

transition matrix depends here on the number of molecules within the simulation box, because the energy change per molecule due to a single particle move is smaller the larger the number of molecules. Two aspects need to be considered for determining an appropriate bin width: the time it takes to visit all bins and the probability to jump between neighboring bins, which is necessary for the calculation of the transition matrix elements. If the binning is chosen too coarse, it may take a long time to visit the highest and lowest energy bins, and it is likely to stay within a bin for many particle moves. If the binning is too fine, it takes a long time to accumulate a sufficient number of measurements for each bin, and it is likely to jump to a distant and not a neighboring bin. Thus, the energy bin width is chosen to be antiproportional to the number of molecules. The whole energy range for a cubic simulation box with $L = 10$ is thus divided into approximately 5000 bins, while a box with $L = 15$ has already 22000 energy bins. Once this histogram is flat enough (the value of each bin of the histogram is above 70% of the average value of all bins), the modification factor f is reduced to $f^{1/10}$, the histogram is reset to zero, and the $G(E^*)$ is replaced by the result obtained from the transition-matrix elements [Eq. (6)]. This procedure is repeated until $\ln f = 10^{-8}$.

In the subsequent "collect" stage, detailed balance is obeyed because $G(E^*)$ is not modified anymore. This allows measuring observables in this stage. Additionally, we continue to measure the transition-matrix elements. In this way, the accuracy of the density of states gets continually enhanced by longer simulations, which is not the case when the transition matrix is not considered.

Because the density of states is obtained in the simulations, the canonical average of any thermodynamic observable A can be calculated with

$$\langle A \rangle_T = \frac{\sum_{E^*} \langle A \rangle_{E^*} G(E^*) \exp{(-E^*\beta^*)}}{\sum_{E^*} G(E^*) \exp{(-E^*\beta^*)}}, \qquad (7)$$

where $\langle A \rangle_{E^*}$ is the microcanonical average of A at energy E^*, which is measured during the simulation.

As order parameter S we use the average of the nematic order parameter of each lattice plane orthogonal to the z axis. The nematic order parameter of a lattice plane is defined as the largest eigenvalue of the matrix

$$Q_{ab} = \frac{3}{2N_{xy}} \sum_{i=1}^{N_{xy}} \hat{\omega}_{i,a}\, \hat{\omega}_{i,b} - \frac{1}{2}\delta_{ab} \qquad (8)$$

with the components of the molecular orientations $(a, b) = (x, y, z)$, the number of molecules in each plane N_{xy}, and the Kronecker delta δ_{ab}. For an ordered system where all molecules of each plane are perfectly aligned, $S = 1$ holds while in the isotropic phase $S \to 0$.

To find phase transitions and to determine their order, we use finite-size scaling. From the scalar order parameter and its fluctuations, we obtain the first cumulant $U_1 = \langle S^2 \rangle / \langle S \rangle^2$. This quantity indicates phase transition temperatures because there it gets independent of the system size. Thus, all cumulants (as a function of temperature) for any simulation box size intersect at the transition temperature. Likewise, we calculate the susceptibility related to the order parameter $\chi = V(\langle S^2 \rangle - \langle S \rangle^2)\beta^*$ with the volume of the simulation box $V = N\lambda^3$. Both the susceptibility and the specific heat,

$c_V = k_B(\langle E^{*2} \rangle - \langle E^* \rangle^2)\beta^{*2}/V$, diverge at phase transitions in the thermodynamic limit. At continuous transitions, their behavior is described by critical exponents. We determine those in simulation boxes that are far below the thermodynamic limit and use the scaling of the maxima of χ and c_V for increasing sizes of the simulation box to draw conclusions about the transition type.

A special case of continuous transitions are Berezinskii-Kosterlitz-Thouless transitions (BKT) [38,39]. These transitions are of infinite order and they are observed in thin films. By cooling a system, it changes from isotropic, where the correlation length decays exponentially with the distance, not to a fully ordered system, but rather to a state which has quasi-long-range order, i.e., a correlation length which decays with a power law. This can be identified by the behavior of the order parameter in the quasi-ordered phase, which decreases for an increasing size of the simulation box.

In the case of a first-order phase transition, there is a free energy barrier between the two phases which has its origin in the coexistence of the phases. Due to these two phases, two equally high peaks are found in $P(E^*)$ at the inverse transition temperature β^*_{trans}. Since the free energy is related to the energy probability distribution by $F = -\ln[P(E^*)]J\beta^{*-1}$, we obtain the height of the barrier by

$$\Delta F = \left| \ln \left(\frac{P_{\max_{\beta^*_{\text{trans}}}}}{P_{\min_{\beta^*_{\text{trans}}}}} \right) \right| J\beta^{*-1}_{\text{trans}}. \qquad (9)$$

$P_{\max}$ is here the height of the two maxima and $P_{\min}$ the value of the minimum in between. For convenience we introduce the reduced barrier $\Delta F^* = \Delta F \beta^* J^{-1}$.

Another observable of interest for chiral liquid crystals is the cholesteric pitch Π, which is given in units of the lattice constant λ so that $\Pi^* = \Pi\lambda^{-1}$ is the respective dimensionless quantity. The pitch is defined as the length on which the nematic director does a full rotation. We determine it in two different ways: in the TMWL simulations, we look at the average angle $\langle \phi_B \rangle$ of the self-determined boundary, which is connected to the pitch by

$$\Pi^* = \frac{2\pi L_z}{|\langle \phi_B \rangle \pm n\pi|}\lambda^{-1} \qquad n = 0, 1, 2, \dots, \qquad (10)$$

where n is a number that accounts for possible helix rotations by π that cannot be detected with the angle ϕ_B alone.

The other method we use with the Metropolis algorithm is to determine the director for each molecular plane L_z orthogonal to the z axis. The slope m of the angles $\varphi(L_z)$ between the projections of the directors on the xy plane and some fixed axis gives the pitch

$$\Pi^* = \frac{2\pi}{m\lambda} \qquad (11)$$

and is found by a linear fit of the measured $\varphi(L_z)$.

In addition to pure systems, we study mixtures of two particle species where we follow the approach used in Ref. [40] for systems with mixed chirality parameters. The species in our system have different values for the exponent p in the interaction energy of Eq. (4), and we randomly distribute the molecules of type 1 and 2 within the system given a specified fraction of one of the types. For the interaction

between type 1 and type 2 molecules, we use the effective exponent $p_{12} = (p_1 + p_2)/2$. K^* is the same for both molecule types, and we choose values for it for which the phase transitions in pure systems show a strong potential-width dependence. For each mixed system, defined by K^*, p_1, p_2 and the fraction of p_2 particles x_{p_2}, we perform two simulations with different distributions of molecules of type 1 and 2. In this way, we can roughly estimate how accurate our results are.

III. RESULTS

A. Bulk

We begin with a discussion of the model interaction potential and the resulting low-temperature phase. The pair interaction of the generalized chiral Lebwohl-Lasher (gcLL) model is illustrated in Fig. 1; shown is the interaction energy for a pair of planar particles separated by $\vec{r}_{ij} = \hat{e}_z$ as a function of their enclosed angle. In the achiral case ($K^* = 0$), the minimum energy state is the (achiral) nematic state, where the cholesteric pitch is infinite. As visualized in the figure, the parameter p defines the sharpness of the potential. For large p, almost only aligned particles contribute to the system's energy, so that an increasing p may well be compared to an increasing particle length in continuous hard-body systems. The effect in bulk systems is that the isotropic-nematic transition seems to be more strongly first order (the transition for $p = 2$ is referred to as weakly first order) [17]. For $|K^*| > 0$, the energy minimum shifts to nonzero angles resulting in a chiral nematic (cholesteric) state with finite cholesteric pitch Π^*. The shift of the global minimum is largest for small p and decreases towards zero for large p. However, a second minimum appears for $p \geqslant 13$ (for the shown case of $K^* = 2$; for smaller K^* larger p values are necessary to get a second minimum, e.g., $p \geqslant 17$ for $K^* = 1$, $p \geqslant 30$ for $K^* = 0.1$, and $p \geqslant 38$ for $K^* = 0.01$), resulting in a more complex behavior of the cholesteric pitch. Note that for $K^* > 2$, the
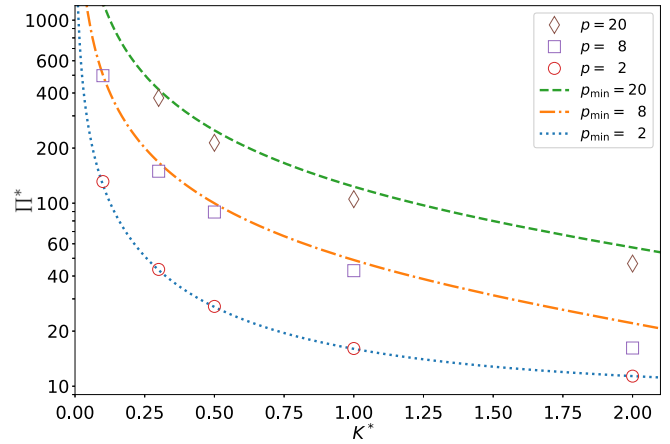
FIG. 2. Cholesteric pitch vs reduced chiral strength for different values of the sharpness parameter p at a reduced inverse temperature well above the isotropic-cholesteric transition, $\beta^* = 1000$. Lines show the results when assuming that only the global interaction minimum contributes to the pitch value. Symbols show results from simulations of a cubic box with length $L = 10$ and self-determined boundary conditions using the Wang-Landau algorithm. Logarithmic y axis.

global minimum is the one at the larger angle, resulting in an unphysically small cholesteric pitch; for $K^* = 2$ and $p \to \infty$, the two minima have the same depth. For very low temperatures (high inverse temperatures), the equilibrium cholesteric pitch is dictated by the global minimum of the pair interaction, $\Pi^* \approx 2\pi/\Delta\phi_{\min}$. But in general, for any nonzero temperature (below the IN* transition), the actual shape and all local minima of the pair interaction contribute to the equilibrium pitch value. We compare the estimates from both global interaction minima and Wang-Landau Monte Carlo simulation, in Fig. 2 for a high inverse temperature $\beta^* = 1000$. The agreement is perfect for $p = 2$; for larger p, the simulation result is slightly below the minimum estimate, in accordance with the change of shape of the interaction potential (Fig. 1) and the small but nonzero temperature. The cholesteric pitch decreases monotonically with increasing chiral strength K^*, and it increases with increasing sharpness parameter p. These trends can be directly inferred from the interaction potential. The chiral part has a minimum at $\Delta\phi = \pi/4$, whereas the achiral part has a minimum at $\Delta\phi = 0$. Thus, the minimum of the total interaction moves from 0 for $K^* = 0$ to $\pi/4$ for $K^* \to \infty$. An increasing p reduces the absolute value of the achiral contribution unless $\Delta\phi = 0$, which leads to a shift of the minimum of the total interaction to smaller angles. For temperatures close to the IN* transition, the pitch deviates from the low-temperature value. We show this in Fig. 3 for two different chiral strengths and the three p values under study. These results are found from Metropolis Monte Carlo simulations, i.e., at fixed temperatures. We chose this algorithm in the context of measuring the cholesteric pitch because the latter is not well defined in disordered systems, which would be included in the Wang-Landau canonical average, Eq. (7). For $p = 2$, the measured pitch weakly fluctuates around the low-temperature value (indicated by the line). In contrast, for larger p, the cholesteric pitch decreases close to the IN* transition to roughly half of its limiting value
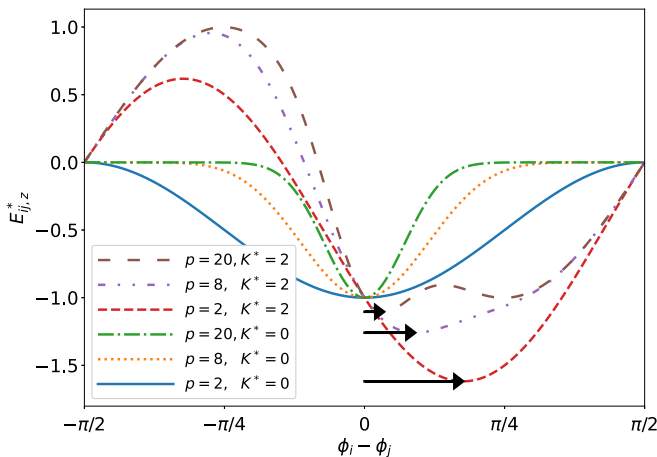

FIG. 1. Pair interaction between particles described by planar vectors with separation $\hat{r}_{ij} = \hat{e}_z$ for different values of the sharpness parameter p and the reduced chiral strength K^*. ϕ_i is the azimuthal angle of the planar vector $\bar{\omega}_i'$. Arrows indicate the shift of the global minimum for $K^* > 0$. For large p a second minimum appears.
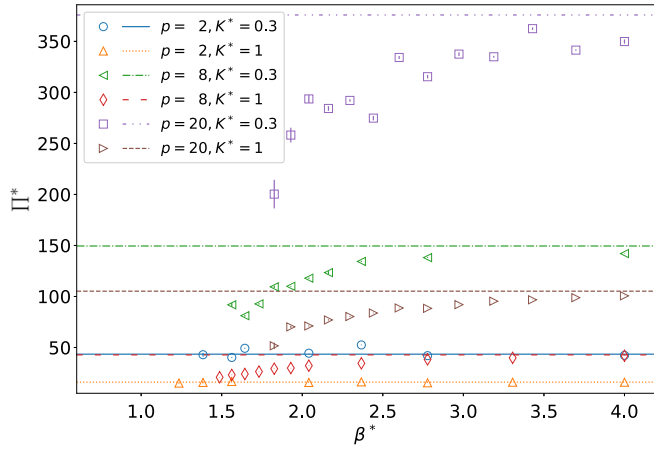
FIG. 3. Cholesteric pitch vs reduced inverse temperature for different values of the sharpness parameter p and the reduced chiral strength K^* close to the isotropic-cholesteric transition. Lines indicate the low-temperature limit, i.e., the results shown in Fig. 2. Symbols show results from simulations of a cubic box with length $L = 10$ and self-determined boundary conditions using the Metropolis algorithm. Error bars depict uncertainties from linear fits of the director's polar angle vs z coordinate.

(indicated by the lines). To explain this behavior, we begin with considering planar particles. For $p = 2$, the potential is symmetric about its minimum at $\Delta\phi = \arctan(K^*)/2$, resulting in $\Pi^* = 4\pi / \arctan(K^*)$ (independent of β^*). For $p > 2$, the potential is not symmetric; the slope in the direction of larger angles is smaller than that in the direction of smaller angles so that the average angle increases with temperature, i.e., the pitch decreases. In our system, the particles are not forced to be planar but may rotate out of the plane. The chiral contribution is then reduced by a factor of $\sin\vartheta_i \sin\vartheta_j$, where ϑ_i the polar angle of particle i. The achiral contribution is reduced whenever $\vartheta_i \neq \vartheta_j$. The effect on the total interaction is, unfortunately, not obvious. To go on, one can compute the polar angle-averaged potential,

$$\overline{E}_{ij} = \frac{\int d\vartheta_i \, d\vartheta_j \, \sin\vartheta_i \sin\vartheta_j \, E_{ij} \exp(-\beta E_{ij})}{\int d\vartheta_i \, d\vartheta_j \, \sin\vartheta_i \sin\vartheta_j \, \exp(-\beta E_{ij})},$$

and study how it changes with temperature. Indeed, we find that the minimum of this potential shifts to slightly larger $\Delta\phi$, supporting the finding of decreasing pitch with increasing temperature. However, the magnitude of the drop of the pitch cannot be explained with the position of the minimum alone. In Ref. [33] the same qualitative behavior (decreasing pitch) is found, and attributed to the gain in orientational entropy due to out-of-plane rotations which increase with temperature.

After discussing the system's behavior in the cholesteric phase, we now turn to the question about the type of the isotropic-to-cholesteric transition. The achiral system ($K^* = 0$) is known to show a first-order IN transition with increasing "strength" for increasing sharpness parameter p [17]. Note that we are here first discussing bulk systems, i.e., $L \times L \times L$ lattice sites with periodic boundary conditions in the x and y direction and self-determined boundary conditions in the z direction. To determine the type of phase transition (or at least rule out certain types), we use finite-size-scaling (FSS)
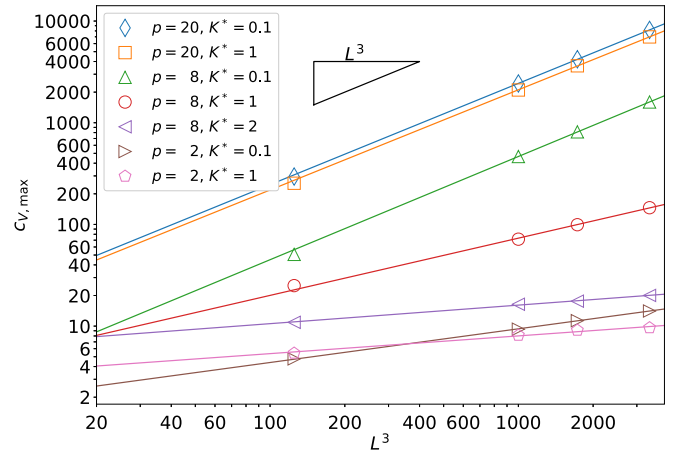

FIG. 4. Maxima of the reduced specific heat vs box "volume" for different values of the sharpness parameter p and the reduced chiral strength K^*. Lines show power-law fits. Logarithmic axes.

analysis. Signs of a first-order phase transition are a linear scaling of the specific heat maxima with the simulation box "volume," L^3, and a linear scaling of the free energy difference (between the two equally high maxima, corresponding to the two phases in coexistence at the transition temperature, and the minimum in between) with the box cross-sectional "area," L^2. We test both relations for different sharpness p and chiral strength K^* and show the respective power-law fits in Figs. 4 and 5.

For $p = 20$, the IN* transition appears to be of first order, independent of the chiral strength. Thus, although the ordered phase is chiral nematic, the nature of the transition is the same as for the achiral case. For less sharp interactions ($p = 8$), the situation changes. The phase transition appears to be of first order only for weak chirality (tested for $K^* = 0.1$); for $K^* \geqslant 1$, we can rule out a first-order transition due to too small power-law exponents. For even smaller p values, no sign of a first-order transition is left, in agreement with previous results [28,32]. Note, however, that in this case, very large system sizes would be needed to draw final conclusions, as
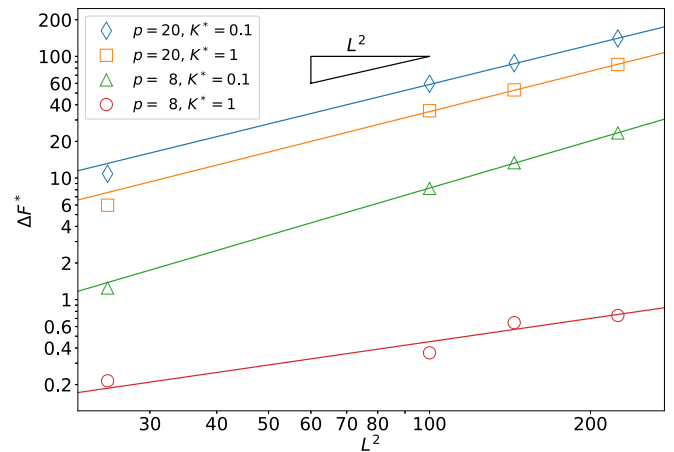

FIG. 5. Reduced free energy difference vs "area" for different values of the sharpness parameter p and the reduced chiral strength K^*. Lines show power-law fits. Logarithmic axes.

TABLE I. Type of IN* transition in bulk systems. † indicates usage of planar particles, i.e., reduced degrees of freedom.

K^* \ p	2	8	20
0.0	Refs. [2–11]: First-order	Ref. [17]: First-order	Ref. [17]: First-order
0.1	—	First-order	First-order
0.725	Ref. [32]: second-order or higher†	—	—
1.0	Ref. [28]: higher than first-order†	Continuous	First-order

$p = 2$ would show only a weak first-order transition. The conclusion of this part is that we can change the nature of the isotropic-cholesteric transition from first order to continuous by enhancing the chiral strength of the interaction potential. The effectiveness of the chiral strength regarding this change does depend on the sharpness of the achiral contribution. Table I summarizes the types of isotropic-cholesteric transitions in bulk systems found in our work and includes literature results, also for the achiral case, for comparison.

B. Two-dimensional limit

The two-dimensional limit (a monolayer film with $L \times L \times 1$) of the Lebwohl-Lasher (and related) models has found much attention during the last decades. Results are controversial as mentioned in the Introduction. The chiral contribution as defined in Eq. (7) does not have an effect in a purely two-dimensional system. Thus, the nature of the transition is that for the achiral case. The mentioned controversy refers to the sharpness parameter $p = 2$, i.e., the original LL model. For $p = 8$, a BKT transition is found by authors who find no transition for $p = 2$ [18,41]. To test the existence of a phase transition, we compute the cumulant U_1 and check for intersections for system sizes $L = 10$, 15, and 20. We use very similar simulation and analysis methods as in Refs. [18,41] but find a BKT transition for both $p = 2$ and 8 indicated by an intersection of the cumulants (cf. Fig. 6 for $p = 2$) and a decrease in the order parameter of the nematic phase for increasing simulation boxes. In addition, we study the case $p = 1$, which, to our knowledge, has not been studied before. Note that this is not equal to the Heisenberg model because of the absolute value used in Eq. (4). We do not find an intersection of the cumulants (cf. Fig. 7) and thus conclude that the system with $p = 1$ does not undergo a phase transition. This finding hints at the origin of the controversy for $p = 2$: The sharpness parameter tunes the type of the phase transition from no transition to a BKT transition to a first-order transition. It is likely that $p = 2$ is just at the border between two types so that different simulation and analysis methods result in different conclusions. The literature results about the types of the isotropic-nematic transition in purely two-dimensional systems are summarized in Table II and appended by our results.
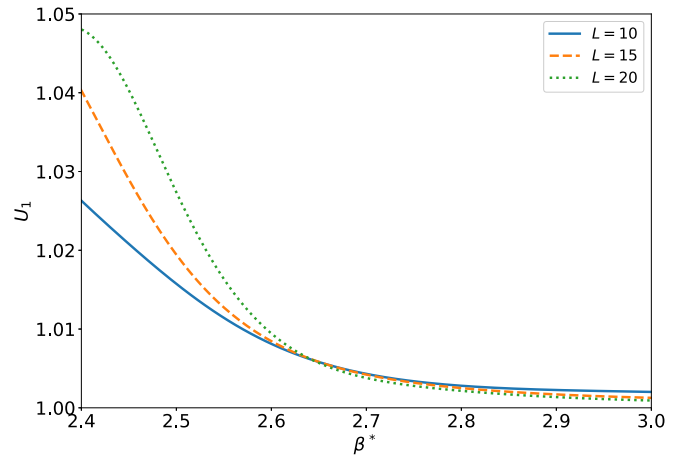

FIG. 6. First cumulants of the order parameter for the exponent $p = 2$ in a monolayer film. At $\beta^* = 2.645(7)$, the cumulants of different simulation box sizes have an intersection, thus indicating a phase transition.

C. Thin system

As stated above, the chirality has no impact in a purely two-dimensional system; we, therefore, study the chirality effect in thin systems of three layers ($L \times L \times 3$) without periodic boundary conditions along the z direction (i.e., free surfaces). For $p = 1$, 2 and 8, we find continuous IN* transitions. For those, we verify the hyperscaling relation, $\overline{\gamma} + 2\overline{\beta} = d = 2$, by fitting power laws to the system size dependence of the susceptibility maxima and the nematic order parameter at the transition, $\chi_{max} \propto L^{\overline{\gamma}}$ and $\langle S_{IN} \rangle \propto L^{-\overline{\beta}}$. Additionally, the exponent of the scaling of the specific heat maxima $\overline{\alpha}$ is much smaller than the dimension of the system so that the transitions cannot be of first order. However, the exponent follows the expected trend of $\overline{\alpha} \to d = 2$ with increasing p, because for $p = 20$, the transition in the thin system is first order (as for the two-dimensional and the bulk limit). We summarize these results in Table III, which includes some literature values for comparison.
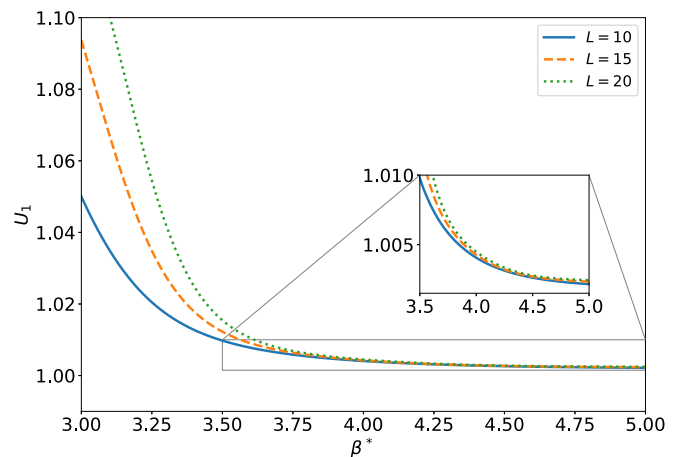

FIG. 7. First cumulants of the order parameter for the exponent $p = 1$ in a monolayer film. In this case there is no intersection, as can be seen in the inset, so that there is no hint at a phase transition.

TABLE II. Type of IN transition in two-dimensional systems. For $p = 2$ the conclusions found in the literature are given in chronological order.

Ref. $\diagdown$ p	1	2	8	20
[12]		No true transition		
[13]		Topological transition		
[14]		BKT		
[8]		No true transition		
[15]		Second-order		
[16]		No quasi-long-range order		
[19]		BKT		
[20]		No critical transition		
[41]		No transition		
[21]		Finite correlation length at finite temperatures		
[22]		No definite conclusion		
[23]		Continuous		
[24]		BKT		
[25]		No quasi-long-range order		
[26]		No finite-temperature transition		
[17]				First-order
[18]			BKT	
This work	No transition	BKT	BKT	First-order

One exception that does not show a transition is the case $p = 8$ and $K^* = 1$, where an intersection of the cumulants for various system sizes is absent. We give a summary of the transition types in Table IV where we do not differentiate between second-order transitions and transitions of BKT type. The reason for this is that we looked at small systems where differentiation between long-range order (second-order transition) and quasi-long-range order (BKT) is not possible with high confidence. For the cases in which we find intersections, we determine the transition temperatures from the intersection points of the cumulants and present them in Table III. The transition temperatures increase with the chiral strength, i.e., chirality enhances the stability of the ordered phase. This originates from the increased energy range that

TABLE IV. Type of IN* transition in thin systems ($L_z = 3$).

K^* $\diagdown$ p	1	2	8	20
0.0	—	Ref. [19]: BKT	Ref. [18]: BKT	Ref. [18]: First-order
0.1	Cont.	Cont.	Cont.	First-order
0.3	Cont.	Cont.	Cont.	First-order
0.5	Cont.	Cont.	Cont.	First-order
1.0	Cont.	Cont.	No transition	First-order

the chiral system can adopt so that the difference in energy between the ordered and the disordered state increases with K^*. By increasing the sharpness parameter p from 2 to 8, the transition temperature decreases, i.e., sharper or steeper interaction potentials enhance the stability of the disordered phase. This can be explained with the larger change in orientational entropy when going from the ordered to the disordered state (the same change in the average potential energy between fully disordered and less disordered state needs a stronger constraint on the orientation of the molecules). On the other hand, by decreasing p from 2 to 1, the transition temperature also decreases, giving another hint at the special role of $p = 2$.

We, thus, have two kinds of change of transition types with sharpness parameter p: (1) from continuous to first-order transition for $K^* = 0.1 - 0.5$ and $p = 8 \to 20$, and (2) from no transition to first-order transition for $K^* = 1$ and $p = 8 \to 20$. Following this, we tested how the system behaves when $p = 8$ and $p = 20$ particles are mixed, as described at the end of Sec. II.

For $K^* = 1$ (no to first-order transition), we compute the cumulants U_1 and find that intersections set in for a fraction of $p = 20$ particles, x_{20}, between 0.2 and 0.4; cf. Fig. 8. That means, a relatively low fraction of particles with a sharp interaction induces an orientational order-disorder phase transition. For $x_{20} \geqslant 0.8$ this transition is of first order.

For $K^* = 0.1$, we see a change of transition type in the scaling of the specific heat maxima. Figure 9 clearly shows that the power-law exponent changes from below 2 to approximately 2 for x_{20} again between 0.2 and 0.4. Thus, also for

TABLE III. Scaling exponents and inverse transition temperatures for the IN* transition in thin systems ($L_z = 3$).

| p, K^*	$\overline{\alpha}$	$\overline{\gamma}$	$\overline{\beta}$	$\overline{\gamma} + 2\overline{\beta}$	$\beta^*_{U_1}$
1, 0.1	0.15(2)	1.5(2)	0.209(6)	1.9(2)	2.01(3)
1, 0.3	0.18(3)	1.60(4)	0.235(3)	2.07(7)	1.926(4)
1, 0.5	0.11(4)	1.64(6)	0.226(6)	2.09(06)	1.863(9)
1, 1.0	0.070(10)	1.70(8)	0.182(3)	2.06(8)	1.721(12)
2, 0.0	—	Ref. [19]: 1.63(3)	—	—	—
2, 0.1	0.20(2)	1.68(12)	0.2110(12)	2.10(12)	1.634(8)
2, 0.3	0.23(2)	1.53(2)	0.240(2)	2.01(2)	1.593(2)
2, 0.5	0.14(2)	1.56(5)	0.232(4)	2.02(5)	1.556(4)
2, 1.0	0.12(2)	1.70(6)	0.197(4)	2.094(6)	1.469(8)
8, 0.0	—	Ref. [18]: 1.71	Ref. [18]: 0.15	Ref. [18]: 2.01	—
8, 0.1	1.25(4)	1.7(2)	0.151(5)	2.0(2)	1.7157(8)
8, 0.3	1.10(5)	1.5(2)	0.181(12)	1.9(2)	1.7086(13)
8, 0.5	0.85(5)	1.57(6)	0.233(4)	2.04(6)	1.6951(7)
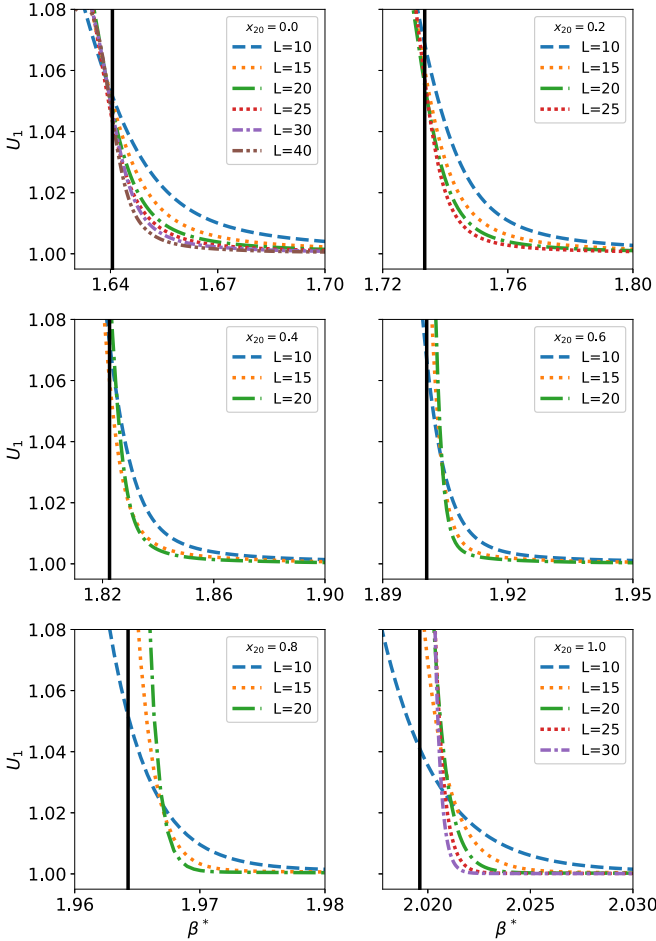
FIG. 8. First cumulants of the order parameter for thin films of mixed systems ($p_1 = 8$, $p_2 = 20$) with a chiral strength of $K^* = 1$. The black vertical line indicates the temperature at which the specific heat of the largest used simulation box has a maximum. This temperature is used as a lower bound for the region where a phase transition can be found. The cumulants at the lowest concentrations of $p = 20$ molecules do not intersect. An intersection can be observed only for concentrations larger than $x_{20} = 0.2$.
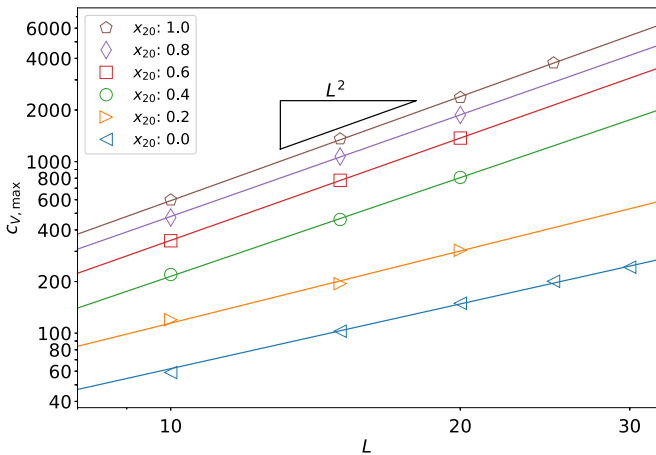

FIG. 9. Maxima of the reduced specific heat vs linear box dimension for $K^* = 0.1$ and different fractions of $p = 20$ particles in a system of $p = 8$ particles. Lines show power-law fits. Logarithmic axes.
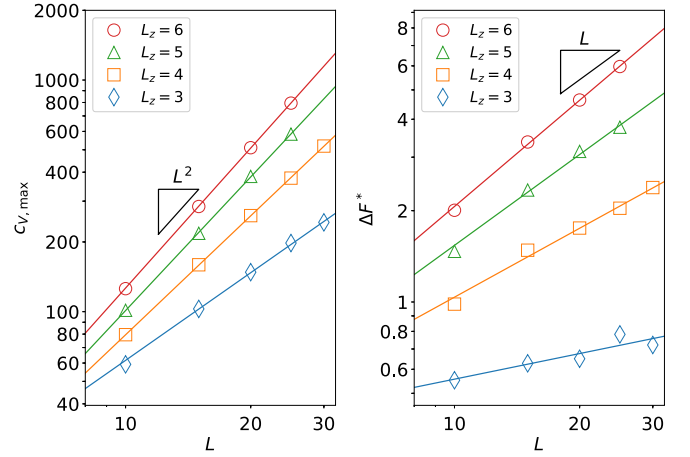

FIG. 10. Maxima of the reduced specific heat (left) and reduced free energy difference (right) vs linear box dimension for $p = 8$ and $K^* = 0.1$ and different box heights L_z. Logarithmic axes.

this case, it is easy to tune the nature of the IN* transition by mixing more and less sharply interacting particles. These findings should be transferable to real systems because the effect of the sharpness parameter might be similar to the effect of an increasing particle length. It would be interesting to see whether this assumption holds.

D. From thin system to bulk

Finally, we discuss the change between the thin system and bulk behavior. Here we use $p = 8$, and the interesting cases are (1) from continuous to first-order transition for $K^* = 0.1$ and (2) from no transition to continuous transition for $K^* = 1$. For the latter, we check again for intersections of the cumulant U_1 and find that L_z must at least be 7 to show a transition. However, the hyperscaling relation is fulfilled only for $L_z = 8$, so that we conclude that for $K^* = 1$, a continuous transition is found for $L_z \geqslant 8$. For $K^* = 0.1$ (continuous to first order), we determine the scaling of the specific heat maxima and the free energy difference. We find a first-order scaling for $L_z = 6$ and $L_z = 5$–6 for specific heat and free energy, respectively, as can be seen in Fig. 10. Thus, the crossover from a continuous to a first-order IN* transition happens for a system thickness between $L_z = 5$ and 6.

IV. CONCLUSION

We have studied the phase behavior of the generalized chiral Lebwohl-Lasher model in bulk and confinement employing Monte Carlo simulations. The ordered phase of this system is a chiral nematic (cholesteric) phase with an equilibrium cholesteric pitch that depends on the details of the interaction potential and, in general, on the temperature. We found that the pitch increases with the sharpness parameter p and decreases with the chiral strength K^*. Close to the isotropic-cholesteric (IN*) transition, the pitch decreases for $p \neq 2$.

We focused on the nature of the IN* transition in dependence of the parameters p and K^* and of the system's geometry. For bulk systems ($L \times L \times L$ with periodic

boundary conditions in all three directions), the transition changes from first order to continuous when the chiral strength increases. In thin systems ($L \times L \times 3$ with periodic boundary conditions only in x and y directions) one can have a first-order transition for large p and a continuous (small K^*) or even no transition (large K^*) for intermediate p. When particles with large and intermediate p are mixed, a change of transition type is found for a fraction of large p particles, x_{20}, between 0.2 and 0.4.

Finally, for $p = 8$, the respective bulk behavior is found for confined systems ($L \times L \times L_z$ with periodic boundary conditions only in x and y directions) with thickness $L_z = 5$–6 for a small chiral strength, and $L_z = 8$ for a large chiral strength. Thus, only very thin systems behave differently from bulk systems regarding the type of the IN* transition.

Adding to the controversial discussion of the quasi-two-dimensional case, we found that $p = 1$ results in the absence of a transition, whereas for $p = 2$ our simulations show a continuous transition. Future studies could include rational values of p to further characterize the continuous to no transition change with p.

Thus, in addition to the previously studied systems with $K^* = 0$ and varying p, or $p = 2$ and varying K^*, we identified further interesting ways to tune the IN* transition in the Lebwohl-Lasher model. The combination of varying p and K^* is also important for studying mixed or doped systems where the involved species could have strongly differing properties.

Our final remark is dedicated to off-lattice models of cholesteric systems. Off-lattice (continuous) systems are more closely related to real systems but are more extensive to study due to the additional positional degrees of freedom. A direct comparison between lattice and off-lattice systems is, for example, given in Ref. [33]. The authors find a very similar behavior of both types of system, e.g., a decreasing cholesteric pitch with increasing temperature. This, however, is different from the behavior found in Ref. [42], where the pitch increases with temperature. The differences in these two examples are the distance dependence of the chiral interaction ($1/r^7$ in [42] vs $1/r^6$ in [33]) and the achiral interaction (hard core repulsion of spherocylinders in [42] vs Lennard-Jones plus aligning interaction in [33]). Besides these two examples, a nonmonotonic behavior of the pitch also is possible, such as found in a theoretical study of hard spherocylinders interacting via a square-well plus chiral potential [43]. Thus, continuous models are not only more expensive to study but also show another variety of possible behaviors. It will be informative to investigate the relation between the gcLL and different off-lattice models in future studies.

[1] M. P. Allen, Molecular simulation of liquid crystals, Mol. Phys. **117**, 2391 (2019).

[2] P. A. Lebwohl and G. Lasher, Nematic-liquid-crystal order—A Monte Carlo calculation, Phys. Rev. A **6**, 426 (1972).

[3] H. J. F. Jansen, G. Vertogen, and J. G. J. Ypma, A Monte Carlo calculation of the nematic-isotropic phase transition, Mol. Cryst. Liq. Cryst. **38**, 87 (1977).

[4] G. Luckhurst and P. Simpson, Computer simulation studies of anisotropic systems, Mol. Phys. **47**, 251 (1982).

[5] U. Fabbri and C. Zannoni, A Monte Carlo investigation of the Lebwohl-Lasher lattice model in the vicinity of its orientational phase transition, Mol. Phys. **58**, 763 (1986).

[6] Z. Zhang, O. G. Mouritsen, and M. J. Zuckermann, Weak First-Order Orientational Transition in the Lebwohl-Lasher Model for Liquid Crystals, Phys. Rev. Lett. **69**, 2803 (1992).

[7] Z. Zhang, M. J. Zuckermann, and O. G. Mouritsen, Phase transition and director fluctuations in the three-dimensional Lebwohl-Lasher model of liquid crystals, Mol. Phys. **80**, 1195 (1993).

[8] P. Pasini, C. Chiccoli, and C. Zannoni, Liquid crystal lattice models I. Bulk systems, in *Advances in the Computer Simulatons of Liquid Crystals*, NATO Science Series, edited by P. Pasini and C. Zannoni (Springer Netherlands, Dordrecht, 2000), pp. 99–119.

[9] D. Jayasri, V. S. S. Sastry, and K. P. N. Murthy, Wang-Landau Monte Carlo simulation of isotropic-nematic transition in liquid crystals, Phys. Rev. E **72**, 036702 (2005).

[10] R. Shekhar, J. K. Whitmer, R. Malshe, J. A. Moreno-Razo, T. F. Roberts, and J. J. de Pablo, Isotropic–nematic phase transition in the Lebwohl–Lasher model from density of states simulations, J. Chem. Phys. **136**, 234503 (2012).

[11] G. Skačej and C. Zannoni, The nematic-isotropic transition of the Lebwohl–Lasher model revisited, Philos. Trans. R. Soc. A **379**, 20200117 (2021).

[12] C. Chiccoli, P. Pasini, and C. Zannoni, A Monte Carlo investigation of the planar Lebwohl-Lasher lattice model, Physica A **148**, 298 (1988).

[13] H. Kunz and G. Zumbach, Numerical evidence for a topological phase transition in a two-dimensional spin model, Phys. Lett. B **257**, 299 (1991).

[14] H. Kunz and G. Zumbach, Topological phase transition in a two-dimensional nematic n-vector model: A numerical study, Phys. Rev. B **46**, 662 (1992).

[15] E. Mondal and S. K. Roy, Finite size scaling in the planar Lebwohl–Lasher model, Phys. Lett. A **312**, 397 (2003).

[16] R. Paredes V. A. I. Fariñas-Sánchez, and R. Botet, No quasi-long-range order in a two-dimensional liquid crystal, Phys. Rev. E **78**, 051706 (2008).

[17] J. M. Fish and R. L. C. Vink, Finite-size effects at first-order isotropic-to-nematic transitions, Phys. Rev. B **80**, 014107 (2009).

[18] J. M. Fish and R. L. C. Vink, Isotropic-to-nematic transition in confined liquid crystals: An essentially nonuniversal phenomenon, Phys. Rev. E **81**, 021705 (2010).

[19] N. G. Almarza, C. Martín, and E. Lomba, Phase behavior of the confined Lebwohl-Lasher model, Phys. Rev. E **82**, 011140 (2010).

[20] A. I. Farinas-Sánchez, R. Botet, B. Berche, and R. Paredes, On the critical behaviour of two-dimensional liquid crystals, Condens. Matter Phys. **13**, 13601 (2010).

[21] Y. Tomita, Finite-size scaling analysis of pseudocritical region in two-dimensional continuous-spin systems, Phys. Rev. E **90**, 032109 (2014).

[22] S. Shabnam, S. DasGupta, and S. K. Roy, Existence of a line of critical points in a two-dimensional Lebwohl Lasher model, Phys. Lett. A **380**, 667 (2016).

[23] B. K. Latha and V. S. S. Sastry, Two Phase Transitions in the Two-Dimensional Nematic Three-Vector Model with No Quasi-Long-Range Order: Monte Carlo Simulation of the Density of States, Phys. Rev. Lett. **121**, 217801 (2018).

[24] Y. Ozeki, A. Matsuda, and Y. Echinaka, Dynamical scaling analysis of phase transition and critical properties for the RP^2 model in two dimensions, Phys. Rev. E **99**, 012116 (2019).

[25] G. Delfino, Y. Diouane, and N. Lamsen, Absence of nematic quasi-long-range order in two-dimensional liquid crystals with three director components, J. Phys. A: Math. Theor. **54**, 03LT01 (2021).

[26] C. Bonati, A. Franchi, A. Pelissetto, and E. Vicari, Asymptotic low-temperature behavior of two-dimensional RP^{N-1} models, Phys. Rev. D **102**, 034513 (2020).

[27] R. L. C. Vink, Liquid Crystals in Two Dimensions: First-Order Phase Transitions and Nonuniversal Critical Behavior, Phys. Rev. Lett. **98**, 217801 (2007).

[28] R. Memmer and F. Janssen, Computer simulation of chiral liquid crystal phases, J. Chem. Soc., Faraday Trans. **94**, 267 (1998).

[29] R. Memmer and O. Fliegans, Microcanonical equilibrium properties of chiral liquid crystals—A Monte Carlo study, Mol. Phys. **101**, 1829 (2003).

[30] J. Saha, B. Nandi, P. K. Mukherjee, and M. Saha, Monte-Carlo simulation of the cholesteric phase in liquid crystals, Mol. Cryst. Liq. Cryst. Sci. Technol. A **250**, 185 (1994).

[31] J. Saha and M. Saha, A lattice model Monte Carlo simulation of cholesteric liquid crystal with freely rotating molecules, Mol. Simul. **19**, 227 (1997).

[32] G. R. Luckhurst, S. Romano, and H. B. Zewdie, Computer simulation studies of anisotropic systems. Part 25.—Chiral nematics, the Dzyaloshinsky–Moriya model, J. Chem. Soc. Faraday Trans. **92**, 1781 (1996).

[33] R. A. Skutnik, J-C. Eichler, M. G. Mazza, and M. Schoen, The temperature dependence of the helical pitch in a cholesteric liquid crystal, Mol. Phys. **119**, e1881638 (2021).

[34] W. M. Saslow, M. Gabay, and W.-M. Zhang, "Spiraling" Algorithm: Collective Monte Carlo Trial and Self-Determined Boundary Conditions for Incommensurate Spin Systems, Phys. Rev. Lett. **68**, 3627 (1992).

[35] N. Metropolis, A. W. Rosenbluth, M. N. Rosenbluth, A. H. Teller, and E. Teller, Equation of state calculations by fast computing machines, J. Chem. Phys. **21**, 1087 (1953).

[36] J.-S. Wang and R. H. Swendsen, Transition matrix Monte Carlo method, J. Stat. Phys. **106**, 245 (2002).

[37] M. S. Shell, P. G. Debenedetti, and A. Z. Panagiotopoulos, An improved Monte Carlo method for direct calculation of the density of states, J. Chem. Phys. **119**, 9406 (2003).

[38] V. L. Berezinskii, Destruction of long-range order in one-dimensional and two-dimensional systems possessing a continuous symmetry group. II. Quantum systems, Sov. Phys. JETP **34**, 610 (1972).

[39] J. M. Kosterlitz and D. J. Thouless, Ordering, metastability and phase transitions in two-dimensional systems, J. Phys. C **6**, 1181 (1973).

[40] R. Memmer and F. Janssen, Computer simulation of chiral liquid crystal phases IX. Chiral nduction in guest-host systems—Calculation of the helical twisting power, Z. Naturforsch. A **54**, 747 (1999).

[41] J. Fish, Phase behavior of liquid crystals in confinement, Ph.D. thesis, University of Göttingen, 2012.

[42] S. Varga and G. Jackson, Simulation of the macroscopic pitch of a chiral nematic phase of a model chiral mesogen, Chem. Phys. Lett. **377**, 6 (2003).

[43] H. H. Wensink and G. Jackson, Generalized van Der Waals theory for the twist elastic modulus and helical pitch of cholesterics, J. Chem. Phys. **130**, 234911 (2009).